RECENT ACCUMULATION OF WATER ICE AT THE NORTH POLE OF MARS? J. Bapst[1,2], S. Byrne[1], J. L. Bandfield[3], [1]Lunar and Planetary Laboratory, University of Arizona, Tucson, AZ, 85721. [2]Dept. of Earth and Space Sciences, University of Washington, Seattle, WA, 98195. [3]Space Science Institute, Boulder, CO, 80301.

Introduction: The polar regions of Mars host Polar Layered Deposits (abbreviated as NPLD for the north) that are up to ~3 km-thick sequences of water ice with varying degrees of dust [1]. The spatial extent of the NPLD is substantial, extending equatorward from the pole to roughly 80ºN, at all longitudes. Both PLDs are thought to have formed over the recent geologic past (~10^6-10^8 yr; [2-6]), where climate change is expected to be driven by changes in orbital elements [7].

The northern residual cap (NRC) spans a large fraction of the NPLD extent. The NRC is composed of water ice and is on the order of a meter thick, though likely exhibits some regional heterogeneity [8]. Several studies have analyzed NRC albedo, composition and morphology; yet comparably few have addressed its thermophysical state (e.g., [9]) and none have addressed how its properties change with depth.

The focus of this study is the physical nature of the NRC, or what we consider the most-recent and potentially-active layer of the NPLD. We investigate how relevant properties (e.g., density, albedo) vary, both laterally, and vertically into the subsurface. The NRC interacts strongly with the current climate, e.g., supplying almost all atmospheric water vapor in summer [10]. Past residual caps (now layers within the NPLD) were also likely to have been strongly influenced by past climates. Thus, understanding the thermal properties of the NRC can inform us of the potential link between climate and polar geology.

Methods: Constraining the thermophysical properties of today's NRC is achieved using observed temperatures and a number of thermal model simulations (sensitive to <5 m). Many studies have used observed temperatures and thermal modeling to derive depth-dependent properties [11-17]. Here use derived temperatures acquired by the Thermal Emission Spectrometer (TES) aboard Mars Global Surveyor (MGS). MGS was operational over four Mars Years (MY), specifically MY24-28. MGS's primary science orbit was inclined approximately 93°, which resulted in high data density near the poles, useful for the study of polar surface properties. Unfortunately, it also resulted in a region of low-to-zero data density poleward of 87°N. Queried data are separated into 10 by 10 km bins for fitting. We used all available TES data that did not share a 'bad' nadir opacity rating [18]. We ignored bins with less <100 observations. Almost all bins are above this threshold, and many near the pole have >1000 observations per bin.

Best-fit properties are determined by calculating a reduced-χ^2 statistic between the observed and model temperatures (see [19]). All observations within a single bin are fit simultaneously, but is restricted by a prescribed seasonal window (here L_S=110-270º). This window is necessary to avoid springtime data which can result in erroneous derivations.

Depth-density Relationships: How density varies with depth constrains key conditions (e.g., ice accumulation rate), and thus aids in understanding how climate affects polar stratigraphy. Predicted depth-density profiles are especially sensitive to the accumulation rate [20]. In addition to a homogeneous case (constant properties with depth), we explore three relationships of depth versus density, in order to compare the near-surface structure of the NRC with predicted profiles of accumulating ice on Mars. The three depth-density relationships explored are abrupt changes in density (e.g., ice table), and exponentially- and linearly-increasing density with depth. The range of these properties in our lookup tables is shown in Table 1. For depth-dependent cases the value of 'Porosity' represents the porosity at the surface, as this value varies with depth.

Results: Because our model is customized to retrieve the thermal properties of porous ice, our results over regolith-covered surfaces should be ignored. For clarity, bins with derived thermal inertia (TI)<800 J m^{-2} K^{-1} $s^{-1/2}$ and derived albedo <0.45 are masked out in the following figures, with the exception of albedo maps.

For the homogeneous case, derived TI is relatively high (≥1000 J m^{-2} K^{-1} $s^{-1/2}$) across the NRC and its outliers (Fig. 1). Derived albedo of the NRC is consistent with the pattern of observed albedo across the NRC (Christensen, 2001), but differs substantially in absolute value (derived albedo being ~0.2 higher).

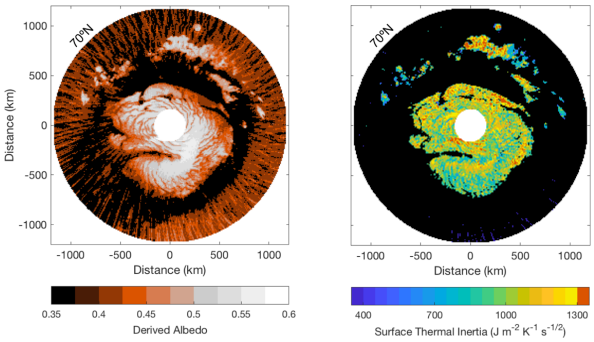

Figure 1. Derived albedo and TI for the north polar region of Mars above 70ºN for the depth-homogeneous case.

Table 1. Lookup Table Elements

Parameter	Range
Latitude	70-90° in 0.5° increments
Albedo	0.1-0.3 in 0.05 increments 0.3-0.6 in 0.025 increments
Porosity	0-0.95 in 0.05 increments (equivalent to thermal inertia range of ~50-2200 J m^{-2} K^{-1} $s^{-1/2}$)
Abrupt Change to Pure Ice (zero porosity)	Depth to pure ice of 0.025, 0.05, 0.1, 0.2, 0.5, 1, 2, and 5 m
Exponentially Decreasing Porosity	e-folding depths of 0.05, 0.1, 0.2, 0.5, 1, 3, and 5 m
Linearly Decreasing Porosity	Porosity gradient of 0.1 to 1 m^{-1} in 0.1 m^{-1} increments

For cases where we include depth-dependent properties, we find we find that the interior of the NRC (i.e., the highest-albedo region) exhibits lower surface TI (~600-800 J m^{-2} K^{-1} $s^{-1/2}$) than the edges of the NRC (Fig. 2). A higher TI annulus varies in width from 10s of km to 100s of km. It is characterized by lower albedo (Fig. 3) and higher surface TI (≥1000 J m^{-2} K^{-1} $s^{-1/2}$). We do not show derived albedo but it is similar to the homogeneous case. The icy outliers span a range of surface TI (~700-900 J m^{-2} K^{-1} $s^{-1/2}$), and are therefore more similar to the NRC interior than its edges (they also share a similarly high albedo).

The high-albedo interior of the residual cap is consistent with a porous layer at the surface (~40-60% porosity), which densifies with depth into a pure-ice layer (0% porosity), within the upper 0.5-1 m. The edge of the residual cap exhibits denser ice, with derived porosities of 20-40% and lower albedo.

Conclusions: Here, we investigated the thermophysical nature of the upper-most layer of the NPLD, the NRC, with emphasis on depth-density relationships within the subsurface (depths of a few meters). We find a strong depth dependence associated with the brightest regions of the NRC interior (i.e., a more-porous layer of ice overlying a denser layer). We interpret this as a result of recent accumulation. This change in density occurs typically within 1 m of the surface. At the edges of the NRC we derive a more-homogeneous subsurface that is denser, and likely older, ice. We interpret this ice as having recently undergone ablation, which is consistent with, and may help explain, its lower albedo.

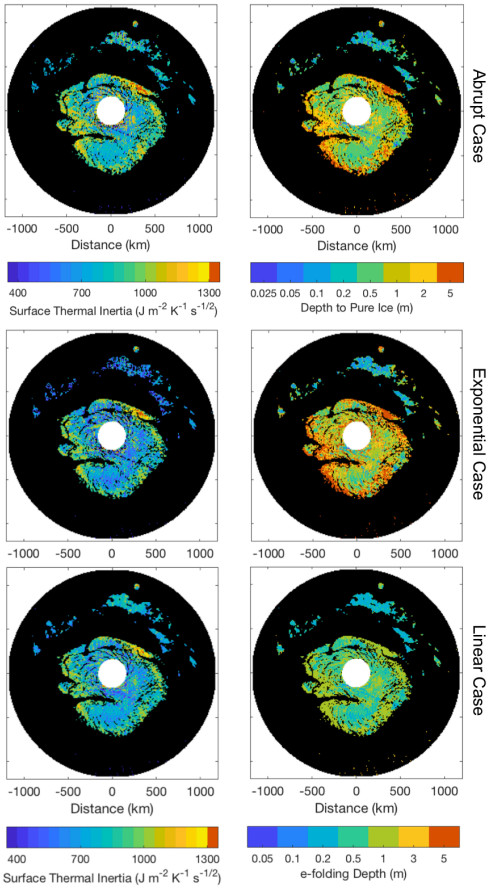

Figure 2. Best-fit albedo, surface TI, and depth-dependence for the three cases explored. The depth-dependence plots have low surface TI regions masked out (black). The linear case of depth-dependence is expressed as an e-folding depth for easy comparison to the exponential case.

References: [**1**] Byrne, S. (2009) *Annu. Rev. Earth Planet. Sci.* **37,** 535–560 [**2**] Levrard, B., et al. (2007) *JGR Planets* **112,** 1–18. [**3**] Phillips, R. J. *et al.* (2008) *Science* **320,** 1182–1185. [**4**] Greve, R. et al. (2010) *Planet. Space Sci.* **58,** 931–940. [**5**] Hvidberg, C. S. *et al.* (2012) *Icarus* **221,** 405–419. [**6**] Smith, I. B. et al. (2016) *Science* **352,** 1075–1078. [**7**] Laskar, J., et al. (2002) *Nature* **419,** 375–377. [**8**] Herkenhoff, K. E, et al. (2007) *Science* **317,** 1711–1715. [**9**] Paige, D. A., et al. (1994) *JGR* **99,** 25959. [**10**] Smith, M. D. (2008) *Annu. Rev. Earth Planet. Sci.* **36,** 191–219. [**11**] Mellon, M. T., et al. (2004) *Icarus* **169,** 324–340. [**12**] Putzig, N. E. and Mellon, M. T. (2007) *Icarus* **191,** 68–94. [**13**] Bandfield, J. L. (2007) *Nature* **447,** 64–67. [**14**] Bandfield, J. L. and Feldman, W. C. (2008) *JGR Planets* **113,** E08001. [**15**] Vasavada, A. R. *et al.* (2012) *JGR. Planets* **117**. [**16**] Hayne, P. O. *et al.* (2017) *JGR Planets*. doi:10.1002/2017JE005387 [**17**] Putzig, N. E. *et al.* (2014) *Icarus* **230,** 64–76. [**18**] Christensen, P. R. *et al.* (2001) *JGR Planets* **106,** 23823–23871. [**19**] Bapst, J., Byrne, S. & Brown, A. J. (2017) *Icarus* doi:10.1016/j.icarus.2017.10.004 [**20**] Arthern, R. J., et al. (2000) *Icarus* **144,** 367–381.